ORIGINAL ARTICLE

Timing differences between HFOs and interictal epileptiform discharges generated in vitro by different mechanisms in rat hippocampal slices: A novel approach

Konstantinos Kalogeropoulos (iD) | **Dimitrios Kleidonas** | **Caterina Psarropoulou** (iD)

Laboratory of Animal and Human Physiology, Department of Biological Applications and Technology, Faculty of Health Sciences, University of Ioannina, Ioannina, Greece

Correspondence
Konstantinos Kalogeropoulos, Bulevar Maršala Tolbuhina 33, New Belgrade, 11070 Belgrade, Serbia.
Email: kost.kalogeropoulos@gmail.com

Present address
Dimitrios Kleidonas, Department of Neuroanatomy, Faculty of Medicine, Institute of Anatomy and Cell Biology, University of Freiburg, Freiburg, Germany

Caterina Psarropoulou, Department of Biological Applications & Technologies, University of Ioannina, Ioannina, Greece

Abstract

Objective: To investigate the effect of generating mechanism on the relationship between interictal-like epileptiform discharges (IEDs) and the underlying High Frequency Oscillations (HFOs; Ripples, R, and Fast Ripples, FR).

Methods: Synchronous spontaneous IEDs were recorded from the CA1 area of hippocampal slices from adult rats, perfused by Mg^{2+}-free ACSF (n = 41slices/14 animals) or 4-aminopyridine ($50\,\mu M$, n = 37slices/16 animals); IED filtering revealed Rs and FRs and several metrics were calculated and compared (amplitude, duration, relative onset, time lag, % overlap, peak frequency, peak power, FR/R).

Results: Longer IEDs and higher 1st Population Spike (PS) amplitude in Mg^{2+}-free ACSF (vs 4-AP; $P < .001$, $P < .001$) correlated with longer duration and higher amplitude Rs ($P < .0001$, $P = .001$) and longer duration FRs ($P < .001$). In both media, Rs and FRs appeared before IED onset with Rs preceding FRs; R- and FR-IED lag ($P = .008$, $P = .01$) as well as R-FR lag ($P = .04$) were significantly longer in Mg^{2+}-free ACSF vs in 4-AP. R peak frequency and power were higher in Mg^{2+}-free ACSF, while no such differences were observed in FRs. Inter-model differences were mostly reflected in Rs, not FRs, suggesting that mechanisms unique to R generation are more active in Mg^{2+}-free ACSF vs in 4-AP. FRs appeared to contribute equally to IEDs irrespective of generating mechanism.

Significance: Several of the metrics used, particularly those regarding the timing between HFOs and IEDs, appear to correlate with the synchronizing mechanism and we propose that they may be useful when investigating antiepileptic substance effects on neuronal network activity.

KEYWORDS
brain, epileptiform discharges, fast, high frequency oscillations, interictal discharges, ripples, seizures

1 | INTRODUCTION

In the adult rodent brain, perfusion with Mg^{2+}-free ACSF (i.e., where Mg^{2+} salts have been omitted) or with a low 4-AP concentration (usually $50\,\mu M$) generate interictal-like discharges (IEDs) which are then used to investigate seizure onset, arrest, or propagation as well as the antiepileptic potential of experimental substances. These in vitro models are often used in parallel, as data obtained with one of them are not predictive of results with the other.

Filtering electrophysiological recordings obtained in vitro has revealed High Frequency Oscillations (HFOs) coinciding with IEDs,[1–4] that is, Ripples (Rs, 80–200 Hz) and Fast Ripples (FRs, 200–600 Hz), which are frequency bands obtained also in EEG recordings. HFOs are an integral part of normal brain function,[5] including memory,[5–7] however, specific HFO types have been linked to specific seizure types or discharges.[8] Rs and FRs have been recorded in acute and chronic models of epileptogenesis both in vivo and in vitro.[2,9–12] Both increase in epileptic tissue[13–15] and their FR/R ratio increases as well.[16] Rs are believed to reflect the interaction between pyramidal cells and interneurons.[17–21] FRs depend on both intrinsic and synaptic neuronal properties, are blocked by excitatory transmission blockers[12] and they may reflect pathological hypersynchronous population spikes of bursting pyramidal cells.[10,12,17] HFOs are potential "biomarkers" and recently their participation in therapeutic schemes has been considered.[22]

In our previous work, we have established that IED changes do not always coincide with parallel HFO changes, following lesions or substance perfusion.[3,4] In this work, we have built upon these findings by focusing on HFO timing relative to IEDs and by using several metrics, some used for the first-time in vitro experiments. We employed two perfusion media, Mg^{2+}-free ACSF and 4-AP, to investigate whether the R-FR-IED relationship depends on the synchronizing mechanism in a measurable way, which would allow us to recommend the use of these metrics in in vitro experiments, with potential applications in the investigation of synchronization mechanisms or the evaluation of antiepileptic substances. To the best of our knowledge, measurements of timing between IEDs and HFOs (relative onset, time lag, percent overlap) have not been undertaken in vitro to date; a single study measuring R onset relative to spikes has been performed based on EEG recordings.[23]

2 | MATERIAL AND METHODS

Experiments were carried out on 30 Wistar rats, 14 of which were used in the Mg^{2+}-free ACSF model and 16 in the 4-AP model. The animals were housed at the University of Ioannina Animal Facility; they had free access to pellet food and water and were exposed to a 12 h light/dark cycle. Animal treatment and experimental procedures complied with ARRIVE guidelines and were conducted in accordance to the Directive 2010/63/EU of the European Parliament and of the Council for animal experiments; they were approved by the Prefectural (Epirus) Animal Care and Use Committee (EL33-BIO01). Throughout this protocol, every care was taken to minimize suffering and the number of animals used.

Hippocampal slices were prepared from adult male animals aged 3 months average (range of 2–6 months). Animals were decapitated under deep ether anesthesia; the brain was quickly removed, and the hippocampi were separated. Transverse 500 -μm thick slices were cut from the middle third of each hippocampus using a McIlwain Tissue Chopper. Throughout the preparation process, the tissue was hydrated or submerged in cool (4°C), oxygenated (95% O_2/5% CO_2) artificial cerebrospinal fluid (ACSF) of the following composition (in mM): NaCl 124, KCl 2, KH_2PO_4 1.25, $CaCl_2$ 2, $MgSO_4$ 2, $NaHCO_3$ 26, glucose 10, at pH 7.4; all reagents were purchased from Sigma. Slices were then placed in two independent Haas-type interface chambers (Haas, Schaerer, and Vosmansky 1979), where they were perfused with 32 ± 1°C warm, oxygenated ACSF containing no added Mg^{2+} (Mg^{2+}-free ACSF, n = 41 slices from 14 animals) or alternatively, $50\,\mu M$ 4-AP (n = 37 slices from 16 animals) and were allowed to equilibrate for at least 1 h before the onset of recording. The volume of each submersion channel was 0.28 mL and the perfusion rate was ~1–2 mL/min. Extracellular recording electrodes (borosilicate glass, filled with 4 M NaCl) were placed in the CA1 hippocampal pyramidal layer. Signals were amplified (AxoClamp 2B or 900A) and stored in a PC using AxoScope software (both from Molecular Devices). After recording stability was ensured (observation periods of >20 minutes), a 3–5 minutes recording was acquired and stored for further analysis, that was conducted offline.

Key Points

- R duration and amplitude and FR duration correlate to those of IEDs.
- Time lags (R-IED, FR-IED, R-FR) depend on generating mechanism.
- R contribute more to IEDs following NMDA-R activation.
- FRs contribute equally to IEDs irrespective of generating mechanism.

Stored recordings (25 kHz/8 kHz anti-aliasing filter) were band-pass filtered at the R (80–200 Hz) and FR (200–600 Hz) frequency ranges using a custom script for Spike2, which applied a Finite Impulse Response (FIR) band-pass digital filter after downsampling the recorded signal by a magnitude of 5. A custom FIR filter was created in Python for each frequency band with a transition gap of 0.5 Hz in its upper bound in order to avoid artifacts in the power spectra. Recorded events in the filtered waveforms were considered HFOs after a visual inspection revealed that they were comprised of at least 4 oscillation cycles measured peak-to-peak.[24,25] HFOs were observed to always coincide temporally with an IED.

The rates of IED recurrence (Hz) and the amplitude of the 1st Population Spike (PS in mV; calculated as the half distance of the two positive peaks to the negative peak) were measured manually. The time points of onset and arrest of IEDs, Rs, and FRs were marked manually. The IED onset was defined as the time point where the signal crossed the baseline before the first PS and the IED arrest as the time point where the signal crossed the baseline after the field EPSP. The time points of R and FR onset and arrest were defined as the points where the signal crossed the baseline before the first and after the last oscillation that was visually distinguishable from the background noise. This was followed by measurements in the time domain, which were taken using a custom script for Spike2. These included the amplitude and duration of the HFOs, the duration of IEDs, the time delay of each band (R, FR) relative to IED onset and to each other, the temporal superimposition of IEDs and Rs or FRs, as well as the percentage of events where the oscillation with the maximal amplitude of the R preceded that of the coinciding FR. The maximal amplitude (referred to simply as amplitude from this point) of Rs and FRs was defined as the amplitude of the waveform at the point of maximal positive deflection from the baseline. The positive peak was chosen as the negative peak usually coincided with the largest IED population spike, which could potentially affect its amplitude A custom script for Spike2 was also used to take measurements in the frequency domain. The power spectrum of each frequency band was calculated with the use of a Fast Fourier Transform (2048 points Hamming window). A novel approach was used to remove the main hum and other baseline noise from the power spectra, without affecting the biological signal being measured. After the initial power spectrum was generated from the summation of 10 events, a spectral analysis of equal duration of the inter-event baseline signal was generated and subtracted from it. Following this, the peak spectral power for each frequency band was measured and the FR/R spectral power ratio was calculated. The custom scripts for the Spike2 software were written by the author KK. A custom FIR filter module for each frequency band was written in Python.

Results are expressed as Mean ± SD. Each sample group was first tested for normality, using a Kolmogorov–Smirnov normality test. Statistical comparisons between sample groups with a normal distribution and equal variance were performed using the two-tailed Student's t-test for unpaired samples, while the effect size was measured using Cohen's d with 95% confidence intervals; In cases where sample groups were characterized by normal distributions but had unequal variances, the Welch's t-test was used instead. The effect size for one-tailed t-test measurements was reported as 95% confidence bounds. Comparisons of sample groups with a nonnormal distribution were performed using the nonparametric Mann–Whitney U-test, while effect size was measured using Cliff's delta with 95% confidence intervals. All statistics were performed using R in the RStudio integrated development environment and Prism 6 (Graphpad Software Inc.). P values >.05 were considered nonsignificant and are not mentioned; P values reflecting one-tailed differences are marked as "1-t". Furthermore, in all Figures P values have been replaced by stars as follows: *$P < .05$, **$P \leq .01$, ***$P \leq .001$, ****$P \leq .0001$.

3 | RESULTS

3.1 | IED features

Perfusion with either Mg^{2+}-free ACSF (n = 41 slices/14 animals) or 4-AP (50 μM, n = 37 slices/16 animals) induced the appearance of synchronous interictal-like discharges (IEDs) composed of a positive field EPSP topped with several Population Spikes (PS; Figure 1A). Quantitative analysis showed that IEDs in Mg^{2+}-free ACSF IEDs had longer duration vs those in 4-AP ($P < .001$, Cliff's delta = −0.698, 95% CI [−0.837, −0.474]), larger 1st PS ($P < .001$, Cliff's delta = −0.432, 95% CI [−0.634, −0.175], see also Figure 2C), and lower frequency ($P < .001$, Cliff's delta = 0.637, 95% CI [0.43, 0.781]). Results are summarized in the upper section of Table 1.

3.2 | High-frequency oscillation features

Filtering the recordings demonstrated that HFOs in the R and FR frequency bands coincided temporally with every IED (Figures 1A,B, 2A). Their characteristics are summarized in the middle (Rs) and lower (FRs) sections of Table 1. Briefly, the mean duration of both Rs and FRs was significantly longer in Mg^{2+}-free ACSF vs 4-AP ($P < .001$, Cohen's d = 1.84, 95% CI [1.35, 2.43] and $P < .001$, Cohen's d = 1.32, 95% CI [0.86, 1.86], respectively; Figure 2B). The amplitude of Rs was larger in Mg^{2+}-free ACSF vs in 4-AP ($P = .001$, Cliff's delta = −0.425, 95% CI [−0.629, −0.167]; Figure 2C).
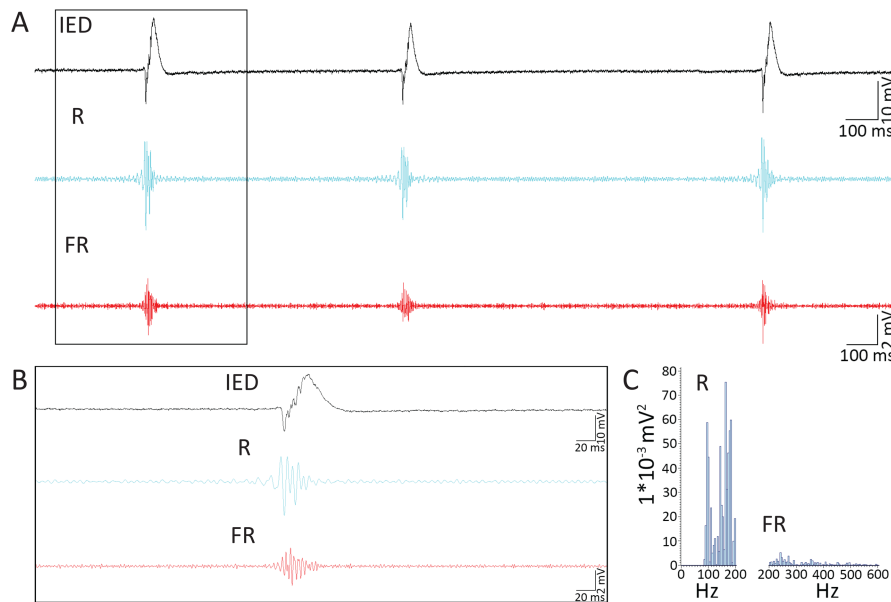
FIGURE 1   IEDs, Rs, and FRs generated by perfusion in Mg^{2+}-free ACSF in the time and frequency domains. A, Unfiltered waveforms of IEDs (top), with the temporally co-occurring Rs (middle) and FRs (bottom). The waveforms of the HFOs were generated through application of a band-pass (R:80–200 Hz, FR:200–600 Hz) FIR filter to the original signal, as described in Methods. B, Expanded view of a single IED and the superimposed Rs and FRs. The same calibration bars apply for both Rs and FRs. C, Power spectra of Rs (left) and FRs (right) generated from n > 10 separated events.

Power spectra generated using a FFT indicated that Rs had significantly higher peak frequency ($P = .03$, one-tailed, Cliff's delta $= -0.256$, 95% CI $[-0.48, -0.001]$) and that the power of the R peak frequency was also significantly higher ($P = .03$, Cliff's delta $= -0.288$, 95% CI $[-0.515, -0.024]$) in Mg^{2+}-free ACSF, whereas for FRs both metrics were similar in the two media.

The temporal overlap between HFOs and IEDs was as follows. Rs (~95% of slices) and FRs (~70% of slices) appeared before IED onset with Rs preceding FRs, in both media. The amount of time (time lag) by which Rs ($P = .008$, Cohen's d $= 0.61$, 95% CI $[0.17, 1.09]$) or FRs ($P = .01$, Cohen's d $= 0.58$, 95% CI $[0.14, 1.06]$) preceded IEDs, as well as this by which Rs preceded FRs ($P = .04$, one-tailed, 95% confidence bound $[-\infty, -1.04 \times 10^{-6}]$) was significantly longer in Mg^{2+}-free ACSF vs in 4-AP. Furthermore, the percentage of IED duration overlapping with Rs was marginally longer in Mg^{2+}-free ACSF ($P = .04$, one-tailed, 95% confidence bound $[-\infty, -0.431]$), however, the percentage of IED duration overlapping with FRs was the same in both media (Table 1).

4 | DISCUSSION

4.1 | IED differences in the two models

Spontaneous IEDs in Mg^{2+}-free ACSF had significantly longer duration, higher amplitude 1st PS, and lower frequency than in 4-AP (see also Ref. [26]), presumably reflecting differences in the respective network synchronization mechanisms in the 2 models. Perfusion with Mg^{2+}-free ACSF generates IEDs mainly via NMDA receptor activation,[27] although secondary mechanisms like the reduction in surface charge screening also play a role.[28,29] In 4-AP, IEDs are primarily a result of the blockade of I_A[30,31] and I_D[32] K^+ currents increasing neuronal excitability and transmitter release[33,34] and are insensitive to NDMA receptor antagonists.[33]

Apparently, the excitation brought about by direct NMDA-R activation generates larger population events compared to the facilitation of transmitter release induced by 4-AP. These then activate long-lasting hyperpolarizing conductances, which may explain the lower IED frequency in Mg^{2+}-free ACSF. Conversely, hyperpolarizing conductances are blocked or diminished in 4-AP, hence the higher IED rates there. The variable activation of interneurons in the two models[35] may also contribute to the observed differences. Currents I_A and I_D (reduced/blocked by 4-AP) are present in all interneuron types,[36–40] so interneuron excitation and contribution to network synchronization in 4-AP might be considered universal. By contrast, interneuron activation in Mg^{2+}-free ACSF is very likely type-specific, as NMDAR subunit composition as well as the ratio between AMPA and NMDA currents varies in interneuron types,[41–48]

4.2 | HFO differences in the two models

The longer IED duration in Mg^{2+}-free ACSF was also reflected in the longer duration of both Rs and FRs.
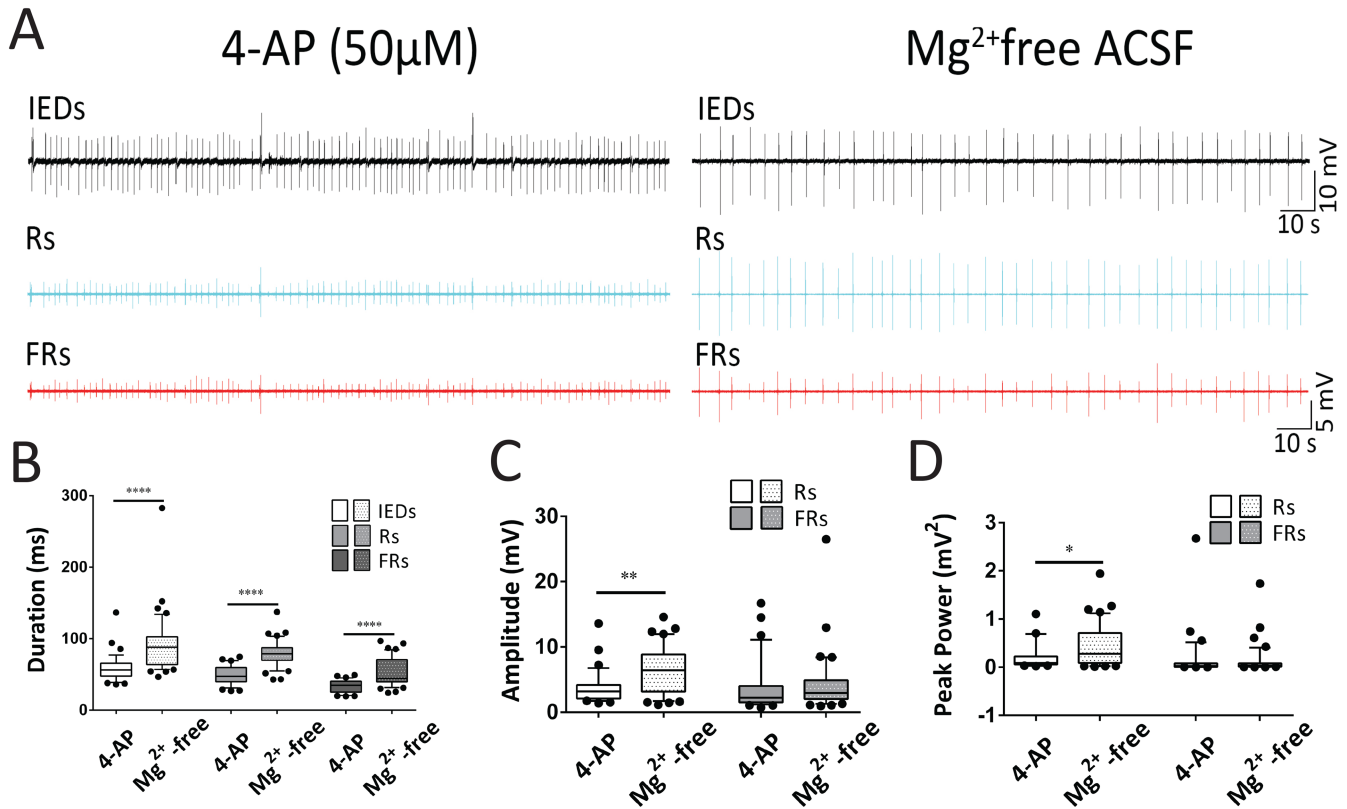
Open Access

FIGURE 2 Traces of IEDs and the underlying HFOs and graphic representation of differences in their characteristics. In the box-and-whiskers plots, the box extends from the 25th to the 70th percentiles while the whiskers are drawn down to the 10th percentile and up to the 90th; dots indicate individual data points; the line in the middle of the box is plotted at the median. A, Low speed records of IEDs and the underlying Rs and FRs from two slices, one on the left bathed in ACSF containing $50\,\mu M$ 4-AP and the other on the right in Mg^{2+}-free ACSF. B, IED, R, and FR duration in the two media. The number of slices was n = 37 in 4-AP and n = 41 in Mg^{2+}-free ACSF; stars indicate ****$P < .001$. C, R and FR peak amplitude in the two media. Number of slices is as in (B); stars indicate **$P = .001$. D, R and FR peak power in the two media. Number of slices is as in (B); stars indicate *$P = .03$.

However, the higher 1st PS amplitude of IEDs was only reflected on the higher R amplitude in the Mg^{2+}-free model, in line to earlier findings, where IED changes were associated to only one band (R or FR) changes.[3,4]

In both models, Rs and FRs were detected earlier than the onset of IEDs reflecting the synchronization mechanisms at play before the onset of synchronous discharges and indicating that HFOs are a precipitating factor bringing about the epileptiform discharges. A similar finding of Rs preceding spikes has been reported in an EEG study.[23] The sequence of their appearance, Rs appearing first followed by FRs (second) and then IEDs (third) was the same in the vast majority of recorded events in both models, suggesting its independence from the generating mechanism. Calculation of the delays between each activity type showed that the R-IED and FR-IED lag were longer in Mg^{2+}-free ACSF (vs in 4-AP), an indication of slower synchronization, in line to the thoughts mentioned earlier about interneuron activation in this model. Computation of IED duration overlapping with Rs or FRs showed longer R-IED overlap in Mg^{2+}-free ACSF (vs

in 4-AP) but similar FR-IED overlap in the two models, an observation suggesting that termination mechanisms may depend on generating mechanisms for Rs but not for FRs.

In the frequency domain, Rs -but not FRs- had a higher peak frequency characterized by higher peak power in Mg^{2+}-free ACSF, indicating their potentiation there. Differences in peak frequency between the two models may reflect the different network configurations generating them in either one.[49] Mathematical models of networks generating Rs and FRs have shown that their peak frequency can be affected by many factors ranging from changes in excitation to inhibition ratio[50] to differences in the innate firing properties of pyramidal neurons.[49] Finally, the FR/R ratio that has been reported to increase in epileptic tissue[16] did not differ between the two models.

In conclusion, several R and FR metrics, most applied for the first time in models of epileptiform discharges in vitro, demonstrated that the timing of HFOs relative to IEDs can be measurably different reflecting neuronal network activating mechanisms. We therefore propose that

TABLE 1 Interictal-like discharge (IED), Ripple and Fast Ripple features recorded in CA1 area of hippocampal slices bathed in Mg^{2+}-free ACSF or in 4-AP (50 μM)

	Mg^{2+}-free ACSF n = 41 slices/14 animals	4-AP ACSF n = 37 slices/16 animals	P-value[*]	Effect size (Cohen's d, Cliff's δ)	95% CI
IEDs					
IED Duration (ms)	92.1 ± 39.5	58.7 ± 18.7	P < .001	δ = −0.698	[−0.837, −0.474]
IED 1st PS Amplitude (mV)	13.9 ± 8.1	8.2 ± 6.1	P < .001	δ = −0.432	[−0.634, −0.175]
IED Frequency (Hz)	0.31 ± 0.21	0.53 ± 0.19	P < .001	δ = 0.637	[0.43, 0.781]
Ripples					
Duration (ms)	79.0 ± 18.3	49.1 ± 13.28	P < .001	d = 1.84	[1.35, 2.43]
Amplitude (mV)	6.4 ± 3.7	3.8 ± 2.5	P = .001	δ = −0.425	[−0.629, −0.167]
Peak frequency (Hz)	147.7 ± 29.5	133.2 ± 31.9	P = .03[1−ta]	δ = −0.256	[−0.48, −0.001]
Peak power (mV^2)	0.408 ± 0.444	0.276 ± 0.571	P = .03	δ = −0.288	[−0.515, −0.024]
R leading IEDs, % of events	94.7 ± 16.6	95.6 ± 11.2			
R-IED lag (ms)	17.9 ± 8.7	13.3 ± 5.9	P = .008	d = 0.61	[0.17, 1.09]
% IED duration coinciding with Rs	71.0 ± 16.8	64.0 ± 18.1	P = 0.04[1−ta]		[−∞, −0.431]
R leading FRs, % of slices	87.3 ± 18.2	91.7 ± 13.5			
R-FR lag (ms)	12 ± 6.1	10 ± 4.8	P = .04[1−ta]		[−∞, −1.04 × 10^{-6}]
Fast Ripples					
Duration (ms)	53.8 ± 8.8	33.1 ± 19.6	P < .001	d = 1.32	[0.86, 1.86]
Amplitude (mV)	4.4 ± 4.4	3.7 ± 3.8			
Peak frequency (Hz)	228.4 ± 27.2	239.7 ± 34.9			
Peak power (mV^2)	0.134 ± 0.307	0.152 ± 0.456			
% IED duration coinciding with FRs	54.7 ± 19.7	51.5 ± 14.8			
FR leading IEDs, % of events	72.3 ± 30.9	68.4 ± 34.6			
FR-IED lag (ms)	8.9 ± 5.7	6.1 ± 3.7	P = .01	d = 0.58	[0.14, 1.06]
FR/R	0.36 ± 0.47	0.45 ± 0.71			

[a]1−t = one-tailed test (student's t-test or M-W U-test).

[*]P values >.05 have been omitted.

these metrics may be useful in investigating network activation in different experimental conditions in vitro and in deciphering the mechanisms of action and antiepileptic potential of pharmacological substances. Another finding of interest is that R generation is more favored in network configurations similar to those created in the Mg^{2+}-free ACSF, thus making it a more appropriate tool for their study.

AUTHOR CONTRIBUTIONS

KK: Data curation, methodology, formal analysis, software, visualization, writing original draft; DK: investigation; CP: conceptualization, project administration, supervision, writing, review and editing.

CONFLICT OF INTEREST

The authors have no competing interests to declare.

ETHICS STATEMENT

The authors affirm that the work described is consistent with the Journal's guidelines for ethical publication.

ORCID

Konstantinos Kalogeropoulos iD https://orcid.org/0000-0002-9750-8374

Caterina Psarropoulou iD https://orcid.org/0000-0002-1929-6951

REFERENCES

1. Staley K, Hellier JL, Dudek FE. Do interictal spikes drive epileptogenesis? Neuroscientist. 2005;11:272–6.
2. Jiruska P, Csicsvari J, Powell AD, Fox JE, Chang WC, Vreugdenhil M, et al. High-frequency network activity, global increase in neuronal activity, and synchrony expansion precede epileptic seizures in vitro. J Neurosci. 2010;30:5690–701.
3. Mikroulis A, Lisgaras CP, Psarropoulou C. Immature status epilepticus: in vitro models reveal differences in cholinergic control and HFO properties of adult CA3 interictal discharges in temporal vs septal hippocampus. Neuroscience. 2018;369:386–98.
4. Lisgaras CP, Mikroulis A, Psarropoulou C. Region-specific effects of early-life status epilepticus on the adult hippocampal CA3 - medial entorhinal cortex circuitry in vitro: focus on interictal spikes and concurrent high-frequency oscillations. Neuroscience. 2021;466:235–47.
5. Buzsaki G, Draguhn A. Neuronal oscillations in cortical networks. Science. 2004;304:1926–9.
6. Igarashi KM. Plasticity in oscillatory coupling between hippocampus and cortex. Curr Opin Neurobiol. 2015;35:163–8.
7. Kucewicz MT, Cimbalnik J, Matsumoto JY, Brinkmann BH, Bower MR, Vasoli V, et al. High frequency oscillations are associated with cognitive processing in human recognition memory. Brain. 2014;137:2231–44.
8. Levesque M, Salami P, Gotman J, Avoli M. Two seizure-onset types reveal specific patterns of high-frequency oscillations in a model of temporal lobe epilepsy. J Neurosci. 2012;32:13264–72.
9. Bragin A, Wilson CL, Almajano J, Mody I, Engel J Jr. High-frequency oscillations after status epilepticus: epileptogenesis and seizure genesis. Epilepsia. 2004;45:1017–23.
10. Bragin A, Engel J Jr, Wilson CL, Fried I, Mathern GW. Hippocampal and entorhinal cortex high-frequency oscillations (100--500 Hz) in human epileptic brain and in kainic acid--treated rats with chronic seizures. Epilepsia. 1999;40:127–37.
11. Bragin A, Wilson CL, Engel J Jr. Chronic epileptogenesis requires development of a network of pathologically interconnected neuron clusters: a hypothesis. Epilepsia. 2000;41(Suppl 6):S144–52.
12. Dzhala VI, Staley KJ. Mechanisms of fast ripples in the hippocampus. J Neurosci. 2004;24:8896–906.
13. Urrestarazu E, Chander R, Dubeau F, Gotman J. Interictal high-frequency oscillations (100-500 Hz) in the intracerebral EEG of epileptic patients. Brain. 2007;130:2354–66.
14. Jirsch JD, Urrestarazu E, LeVan P, Olivier A, Dubeau F, Gotman J. High-frequency oscillations during human focal seizures. Brain. 2006;129:1593–608.
15. Weiss SA, Alvarado-Rojas C, Bragin A, Behnke E, Fields T, Fried I, et al. Ictal onset patterns of local field potentials, high frequency oscillations, and unit activity in human mesial temporal lobe epilepsy. Epilepsia. 2016;57:111–21.
16. Staba RJ, Frighetto L, Behnke EJ, Mathern GW, Fields T, Bragin A, et al. Increased fast ripple to ripple ratios correlate with reduced hippocampal volumes and neuron loss in temporal lobe epilepsy patients. Epilepsia. 2007;48:2130–8.
17. Bragin A, Engel J Jr, Wilson CL, Fried I, Buzsaki G. High-frequency oscillations in human brain. Hippocampus. 1999;9:137–42.
18. Csicsvari J, Hirase H, Czurko A, Mamiya A, Buzsaki G. Oscillatory coupling of hippocampal pyramidal cells and interneurons in the behaving Rat. J Neurosci. 1999;19:274–87.
19. Liotta A, Caliskan G, ul Haq R, Hollnagel JO, Rosler A, Heinemann U, et al. Partial disinhibition is required for transition of stimulus-induced sharp wave-ripple complexes into recurrent epileptiform discharges in rat hippocampal slices. J Neurophysiol. 2011;105:172–87.
20. Jiruska P, Alvarado-Rojas C, Schevon CA, Staba R, Stacey W, Wendling F, et al. Update on the mechanisms and roles of high-frequency oscillations in seizures and epileptic disorders. Epilepsia. 2017;58:1330–9.
21. Ylinen A, Bragin A, Nadasdy Z, Jando G, Szabo I, Sik A, et al. Sharp wave-associated high-frequency oscillation (200 Hz) in the intact hippocampus: network and intracellular mechanisms. J Neurosci. 1995;15:30–46.
22. Takeuchi Y, Berenyi A. Oscillotherapeutics - Time-targeted interventions in epilepsy and beyond. Neurosci Res. 2020;152:87–107.
23. van Klink N, Frauscher B, Zijlmans M, Gotman J. Relationships between interictal epileptic spikes and ripples in surface. EEG Clin Neurophysiol. 2016;127:143–9.
24. Jacobs J, LeVan P, Chander R, Hall J, Dubeau F, Gotman J. Interictal high-frequency oscillations (80-500 Hz) are an indicator of seizure onset areas independent of spikes in the human epileptic brain. Epilepsia. 2008;49:1893–907.
25. Zhou G, Noto T, Sharma A, Yang Q, Gonzalez Otarula KA, Tate M, et al. HFOApp: a MATLAB graphical user interface for high-frequency oscillation marking. eNeuro. 2021;8:ENEURO.0509-20.2021.
26. Jones NA, Hill AJ, Smith I, Bevan SA, Williams CM, Whalley BJ, et al. Cannabidiol displays antiepileptiform and antiseizure properties in vitro and in vivo. J Pharmacol Exp Ther. 2010;332:569–77.
27. Anderson WW, Lewis DV, Swartzwelder HS, Wilson WA. Magnesium-free medium activates seizure-like events in the rat hippocampal slice. Brain Res. 1986;398:215–9.
28. McLaughlin S, Szabo G, Eisenman G. Divalent ions and the surface potential of charges phospholipid membranes. J Gen Physiol. 1971;58:667–87.
29. Hamon B, Stanton PK, Heinemann U. An N-methyl-D-aspartate receptor-independent excitatory action of partial reduction of extracellular [Mg^{2+}] in CA1-region of rat hippocampal slices. Neurosci Lett. 1987;75:240–5.

30. Nakajima Y, Nakajima S, Leonard R, Yamaguchi K. Acetylcholine raises excitability by inhibiting the fast transient potassium current in cultured hippocampal neurons. PNAS. 1986;83:3022–6.

31. Segal M, Barker JL. Rat hippocampal neurons in culture: potassium conductances. J Neurophysiol. 1984;51:1409–33.

32. Storm JF. Temporal integration by a slowly inactivating K+ current in hippocampal neurons. Nature. 1988;336:379–81.

33. Perreault P, Avoli M. Physiology and pharmacology of epileptiform activity induced by 4-aminopyridine in rat hippocampal slices. J Neurophysiol. 1991;65:771–85.

34. Rutecki PA, Lebeda FJ, Johnston D. 4-Aminopyridine produces epileptiform activity in hippocampus and enhances synaptic excitation and inhibition. J Neurophysiol. 1987;57:1911–24.

35. Karlocai MR, Kohus Z, Kali S, Ulbert I, Szabo G, Mate Z, et al. Physiological sharp wave-ripples and interictal events in vitro: what's the difference? Brain. 2014;137:463–85.

36. Zhang L, McBain C. Potassium conductances underlying repolarization and afterhyperpolarization in rat CA1 hippocampal interneurons. J Physiol (Lond). 1995;488:661–72.

37. Zhang L, McBain CJ. Voltage-gated potassium currents in stratum oriens-alveus inhibitory neurones of the rat CA1 hippocampus. J Physiol. 1995;488(Pt 3):647–60.

38. Chikwendu A, McBain CJ. Two temporally overlapping "delayed-rectifiers" determine the voltage-dependent potassium current phenotype in cultured hippocampal interneurons. J Neurophysiol. 1996;76:1477–90.

39. Martina M, Schultz JH, Ehmke H, Monyer H, Jonas P. Functional and molecular differences between voltage-gated K+ channels of fast-spiking interneurons and pyramidal neurons of rat hippocampus. J Neurosci. 1998;18:8111–25.

40. Lien CC, Martina M, Schultz JH, Ehmke H, Jonas P. Gating, modulation and subunit composition of voltage-gated K(+) channels in dendritic inhibitory interneurones of rat hippocampus. J Physiol. 2002;538:405–19.

41. McBain CJ, Dingledine R. Heterogeneity of synaptic glutamate receptors on CA3 stratum radiatum interneurones of rat hippocampus. J Physiol. 1993;462:373–92.

42. Monyer H, Burnashev N, Laurie DJ, Sakmann B, Seeburg PH. Developmental and regional expression in the rat brain and functional properties of four NMDA receptors. Neuron. 1994;12:529–40.

43. Standaert DG, Landwehrmeyer GB, Kerner JA, Penney JB Jr, Young AB. Expression of NMDAR2D glutamate receptor subunit mRNA in neurochemically identified interneurons in the rat neostriatum, neocortex and hippocampus. Brain Res Mol Brain Res. 1996;42:89–102.

44. Lei S, McBain CJ. Distinct NMDA receptors provide differential modes of transmission at mossy fiber-interneuron synapses. Neuron. 2002;33:921–33.

45. Matta JA, Pelkey KA, Craig MT, Chittajallu R, Jeffries BW, McBain CJ. Developmental origin dictates interneuron AMPA and NMDA receptor subunit composition and plasticity. Nat Neurosci. 2013;16:1032–41.

46. von Engelhardt J, Bocklisch C, Tonges L, Herb A, Mishina M, Monyer H. GluN2D-containing NMDA receptors-mediate synaptic currents in hippocampal interneurons and pyramidal cells in juvenile mice. Front Cell Neurosci. 2015;9:95.

47. De Marco Garcia NV, Priya R, Tuncdemir SN, Fishell G, Karayannis T. Sensory inputs control the integration of neurogliaform interneurons into cortical circuits. Nat Neurosci. 2015;18:393–401.

48. Akgul G, McBain CJ. Diverse roles for ionotropic glutamate receptors on inhibitory interneurons in developing and adult brain. J Physiol. 2016;594:5471–90.

49. Fink CG, Gliske S, Catoni N, Stacey WC. Network mechanisms generating abnormal and normal hippocampal high-frequency oscillations: a computational analysis. eNeuro. 2015;2:ENEURO.0024-15.2015.

50. Geisler C, Brunel N, Wang XJ. Contributions of intrinsic membrane dynamics to fast network oscillations with irregular neuronal discharges. J Neurophysiol. 2005;94:4344–61.